Numerical Simulation of Hardness Distribution at the HAZ of P355GH Steel

Mišo Bjelić[1*], Karel Kovanda[2], Ladislav Kolařík[2], Marie Kolaříková[2], Miomir Vukićević[1], Branko Radičević[1]
[1]Faculty of Mechanical and Civil Engineering, University of Kragujevac, Kraljevo (Serbia)
[2]Faculty of Mechanical Engineering, Czech Technical University, Prague (Czech Republic)

Microstructure of the weld seam and the HAZ has an essential impact on different mechanical properties of welded joint. This article presents a methodology for prediction of Vickers hardness in HAZ of welded plates. In order to achieve this goal we have used 3D model of heat transfer during welding, coupled with Kirkaldy's model of austenite decomposition. This coupling have made possible prediction of the volume fractions of ferrite, pearlite and bainite and also prediction of Vickers hardness distribution. Results of simulation run were found to be in reasonable good accordance with experimental ones.

Keywords: Welding, Numerical modeling, Simulation, Microstructure, Hardness

1. INTRODUCTION

Simulation models of welding processes give us an insight into the influence of welding parameters on temperature field in welded parts and by means of temperature fields and the influence to geometry and microstructure of welded joints. Microstructure of welded seam and HAZ has critical impact on mechanical properties of welded joint. Since the first analytical models of Rosenthal [1] and Rykalin [2], complexity of simulation models has grown rapidly [3,4]. But this complexity makes these models unreachable in realistic conditions due to the long time to run the simulation.

Despite good weldability of P355GH steel, it is very important to predict microstructural changes during its welding having in mind that this type of steel is widely used for elevated temperature purposes. Hardness of HAZ which mainly depends on martensite content, has great influence on cracking resistance [5]. Bearing in mind the need to reduce the simulation time, in this article we have coupled an analytical, three-dimensional, quasi-stationary model of heat transfer during GMA welding [6] with Kirkaldy's model [7] of austenite decomposition during cooling stage of welding process. Coupling of these models made us possible to estimate the value of Vickers hardness in the cross section of the welded joint.

2. MODEL OF HEAT TRANSFER

Welding heat source acts in a narrow localized area where a molten pool is formed. Regardless of difficulties, modeling the heat transfer during welding gives us informations about the influence of different process parameters on the heat transfer process itself and also nformations about the influence to the output results that include seam geometry, welded microstructure, deformation, etc.

Quasy-stationary partial differential equation which describes 3-D heat conduction during welding [6] in moving coordinate sistem, fig. 1 is given by (1):

$$-v_z\left(1+\frac{L}{c_p}\frac{\partial f_{liq}}{\partial T}\right)\frac{\partial T}{\partial \xi}=\frac{\lambda}{\rho c_p}\left(\frac{\partial^2 T}{\partial \xi^2}+\frac{\partial^2 T}{\partial y^2}+\frac{\partial^2 T}{\partial z^2}\right)+q_l \quad (1)$$

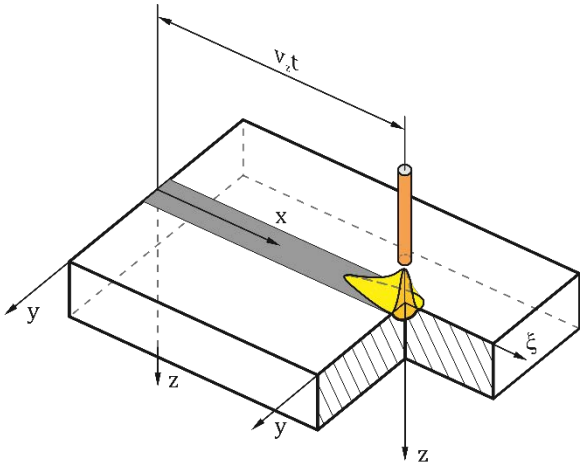

Figure 1:Moving coordinate system

Proportion of the liquid phase can be represented by (2):

$$f_{liq}=\begin{cases}0 & for \quad T\le T_{sol}\\ \dfrac{T-T_{sol}}{T_{liq}-T_{sol}} & for \quad T_{sol}<T<T_{liq}\\ 1 & for \quad T\ge T_{liq}\end{cases} \quad (2)$$

As a heat source model, we have used Goldak's double elliptic model [8]. The feature of this model is that the front half of the model is a part of an ellipsoidal source, while the last half is a part of the second ellipsoidal source. Within the front half of the model, heat density distribution is carried out by (3):

$$q_{lf}(x,y,z)=\frac{6\sqrt{3}f_f Q}{a_{hf}b_h c_h \pi\sqrt{\pi}}e^{-3\frac{x^2}{a_{hf}^2}}e^{-3\frac{y^2}{b_h^2}}e^{-3\frac{z^2}{c_h^2}} \quad (3)$$

The heat density distribution within the last half of the heat source model is described by (4):

*Corresponding author: Dositejeva 19, 36000 Kraljevo, bjelic.m@mfkv.kg.ac.rs

$$q_{lb}(x,y,z)=\frac{6\sqrt{3}f_bQ}{a_{hb}b_hc_h\pi\sqrt{\pi}}e^{-3\frac{x^2}{a_{hb}^2}}e^{-3\frac{y^2}{b_h^2}}e^{-3\frac{z^2}{c_h^2}} \quad (4)$$

It is necessary that the following condition be fulfilled (5):

$$f_f + f_b = 2 \quad (5)$$

On the basis of (1) it may be seen that the calculation of temperatures in welded plates requires knowledge of the values of selected thermo-physical parameters: density, specific heat capacity and thermal conductivity. It is possible to adopt that the values of these parameters are constant, but in real terms this is not the case. In order to calculate temperature distribution in welded plates more accurately, it is necessary to use values of the given parameters as a function of temperature.

3. THERMOPHYSICAL PROPERTIES

In the experimental part of this article we have used P355GH steel with chemical composition shown in Table 1 as a base material and OK Autrod 12.50 wire with chemical composition shown in Table 2 as a filler material. Since it was not possible to found literature data about the density, specific heat capacity and thermal conductivity as a function of temperature temperature, we have used methodology presented in [6,9].

Table 1. Chemical composition of base material

C %	**Si** %	**Mn** %	**Nb** %	**P** %	**S** %
0.20	0.19	1.45	0.014	0.016	0.062

Table 2. Chemical composition of filler material

C %	**Si** %	**Mn** %	**P** %	**S** %
0.08	0.58	1.06	0.009	0.01

Results of density modeling using mentioned methodology can be seen on fig. 2.

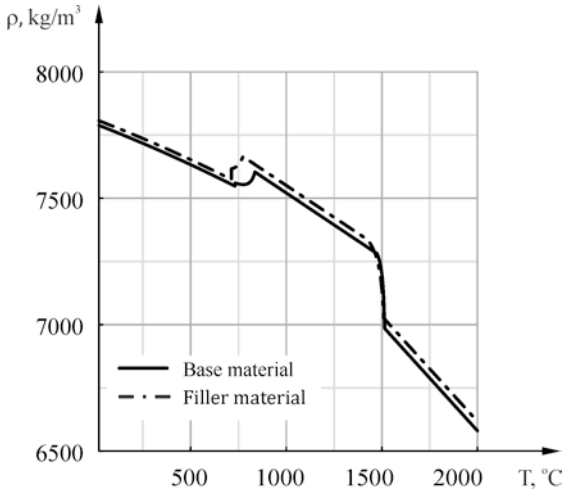

Figure 2: Density of base and filler material vs.temperature

Thermal conductivity and effective heat capacity for base and filler material as a functions of temperature are shown in fig 3 and fig. 4.

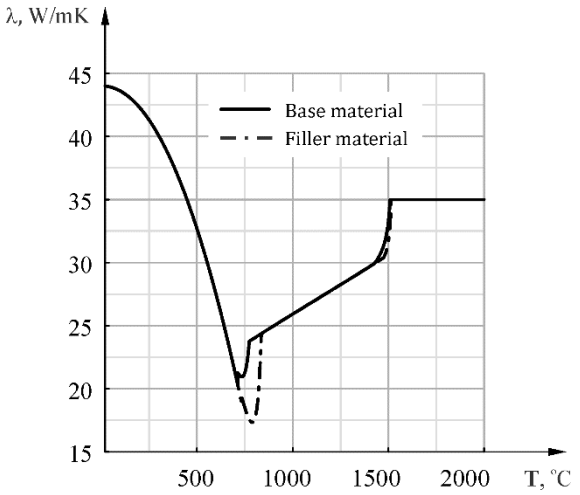

Figure 3: Thermal conductivity of base and filler material vs.temperature

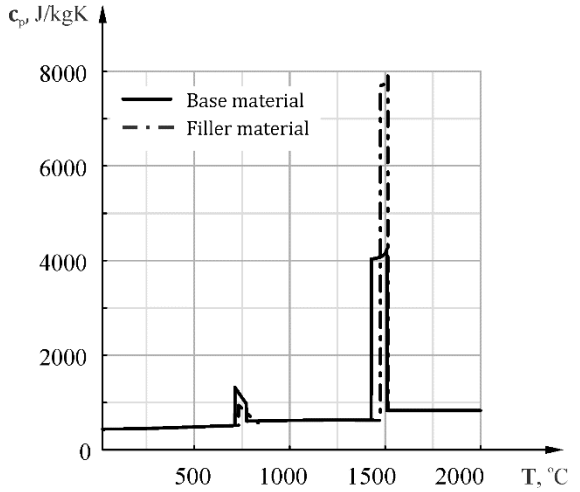

Figure 4: Effective heat capacity of base and filler material vs.temperature

4. MICROSTRUCTURAL MODEL

The microstructure of the welded joint, that is, microstructure of the weld seam and the HAZ, has a crucial effect on the mechanical properties of the welded joint. Description of steel microstucture in practice is most commonly made using austenite isothermal transformation diagrams and the continuous cooling diagrams in welding. For specific steel, these diagrams are obtained by experimental testing. However, in the absence of experimental diagrams for the steel of a particular chemical composition, models which desribe austenitic isotermal transformation process can be used. Based on the research [10,11], Kirkaldy [7] proposed a series of equations which describe kinetics of austenitic isothermal transformation.

For the reaction of the austenite transformation into ferrite under isothermal conditions, the time required for the particular amount X_F of ferrite to be formed can be described as (6):

$$\tau_F = R_F \int_0^X \frac{dX_F}{X_F^{\frac{2(1-X_F)}{3}}(1-X_F)^{\frac{2X_F}{3}}} \quad (6)$$

Simillary, for the reaction of the austenite trasformation into pearlite, Kirkaldy proposed (7):

$$\tau_P = R_P \int_0^X \frac{dX_P}{X_P^{\frac{2(1-X_P)}{3}} (1-X_P)^{\frac{2X_P}{3}}} \quad (7)$$

And for the reaction of the austenite trasformation into bainite (8):

$$\tau_B = R_B \int_0^X \frac{dX_B}{X_B^{\frac{2(1-X_B)}{3}} (1-X_B)^{\frac{2X}{3}}} \quad (8)$$

Coefficients R_F, R_P, R_B are described by (9-11):

$$R_F = \frac{59.6Mn + 1.45Ni + 67.7Cr + 244Mo}{2^{\frac{(G-1)}{2}} \left(Ae_3 - T\right)^3 \cdot e^{\left(\frac{-23500}{RT}\right)}} \quad (9)$$

$$R_P = \frac{1.79 + 5.42\left(Cr + Mo + 4Mo \cdot Ni\right)}{2^{\frac{(G-1)}{2}} \left(Ae_1 - T\right)^3 \cdot D_P} \quad (10)$$

$$R_B = \frac{\left(2.34 + 10.1C + 3.8Cr + 19Mo\right)10^{-4} Z}{2^{\frac{(G-1)}{2}} \left(B_S - T\right)^3 \cdot e^{\left(\frac{-27500}{RT}\right)}} \quad (11)$$

While coefficients Z and D_P can be calculated as (12-13):

$$\frac{1}{D_P} = \frac{1}{e^{\left(\frac{-27500}{RT}\right)}} + \frac{0.01Cr + 0.052Mo}{e^{\left(\frac{-37000}{RT}\right)}} \quad (12)$$

$$Z = e^{\left[X_B^2\left(1.9C + 2.5Mn + 0.9Ni + 1.7Cr + 4Mo - 2.6\right)\right]} \quad (13)$$

Or if following condition (14) is satisfied then value of the coefficient Z is equal to 1.

$$\left(1.9C + 2.5Mn + 0.9Ni + 1.7Cr + 4Mo - 2.6\right) < 0 \quad (14)$$

Based on Kirkaldy's model, we have calculated TTT diagrams for the base material, fig. 5, as well as for filler material, fig. 6, using MATLAB.

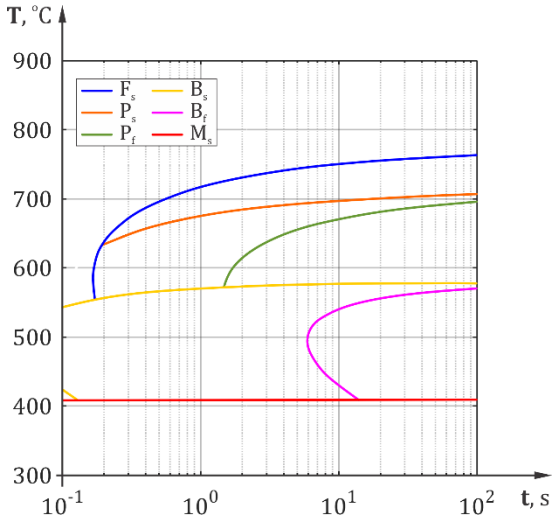

Figure 5: TTT diagram for base material

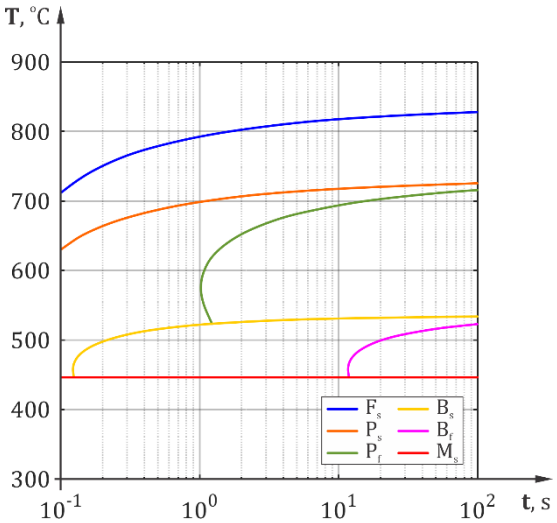

Figure 6: TTT diagram for filler material

5. HARDNESS

Hardness at any point in HAZ depends on the fraction ammount of individual phases: ferrite, X_F, pearlite, X_P, bainite, X_B and martensite, X_M. If we know fraction ammount of each of these phases at a certain point, the hardness can be computed [12] using the equation (15):

$$HV = HV_F \cdot X_F + HV_P \cdot X_P + HV_B \cdot X_B + HV_M \cdot X_M \quad (15)$$

Hardness of the individual phases depends on the chemical composition of the steel and on the cooling rate at 700 ° C [13]. Hardness of ferrite and pearlite can be calculated as (16):

$$H_{FP} = 42 + 223C + 53Si + 30Mn + 12.6Ni + 7Cr + 19Mo + \left(10 - 19Si + 4Ni + 8Cr + 130V\right)\log\left(V_r\right) \quad (16)$$

For the bainite and martensite hardness is calculated based on (17-18):

$$H_B = -323 + 185C + 330Si + 153Mn + 65Ni + 144Cr + 191Mo + \left(89 + 53C - 55Si - 22Mn - 10Ni - 20Cr - 33Mo\right)\log\left(V_r\right) \quad (17)$$

$$H_M = 127 + 949C + 27Si + 11Mn + 8Ni + 16Cr + 21\log\left(V_r\right) \quad (18)$$

Cooling rate at 700°C is described by (19):

$$V_r = 3600\left(\frac{800^o - 500^o}{\Delta t_{8/5}}\right) \quad (19)$$

During the time, grain size increases while the level of increase depends on temperature, activation energy and time [12,14] and can be descibed by (20):

$$\frac{dg}{dt} = \frac{k}{2g} \cdot e^{\left(\frac{-Q}{RT}\right)} \quad (20)$$

Direct application of Kirkaldy’s model in case of welding is not possible because the welding processes take place with variable heating and cooling rates. According to Scheil's additivity rule [15], fig 7, during continous cooling, austenite decomposition starts when the following condition is fulfilled (21):

$$\sum_{j=1}^{m} \frac{\Delta t_j}{\tau_j} = 1 \qquad (21)$$

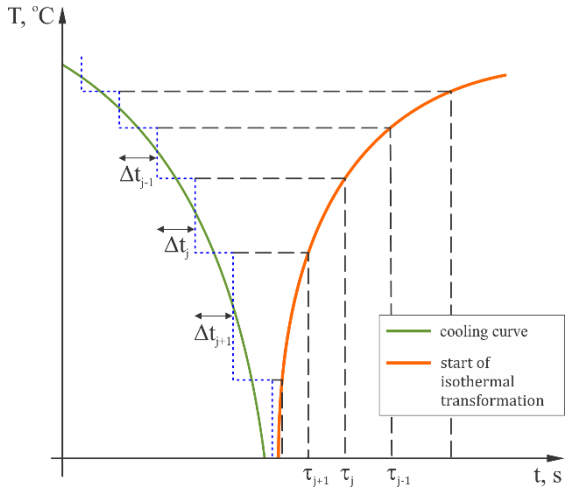

Figure 7: Scheil's additivity rule

6. SIMULATION

The simulation was conducted with following welding parameters: welding current I = 221.1 A, arc voltage U = 21.9 V, welding speed v_w = 0.008 m/s, temperature of plate Tp = 22°C, and atmosphere temperature, Ta = 20.5 °C. Results of simulation are shown of figs.8 - 12.

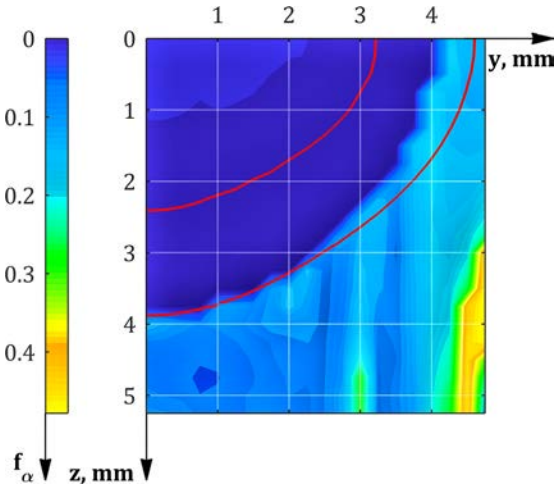

Figure 8: Simulation of ferrite volume fraction

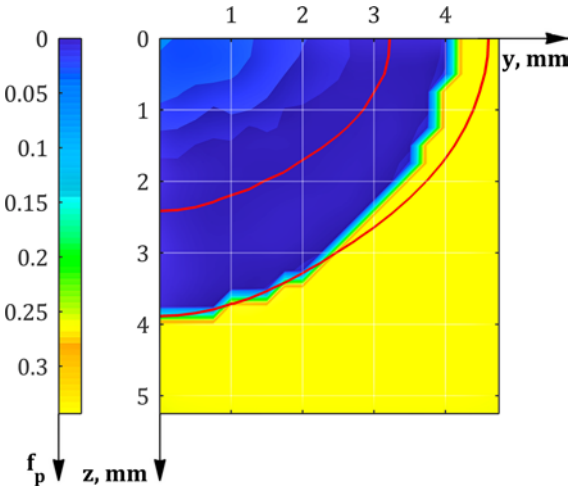

Figure 9: Simulation of pearlite volume fraction

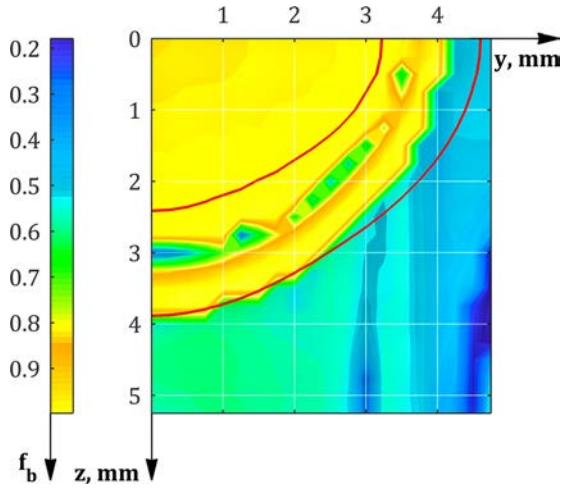

Figure 10: Simulation of bainite volume fraction

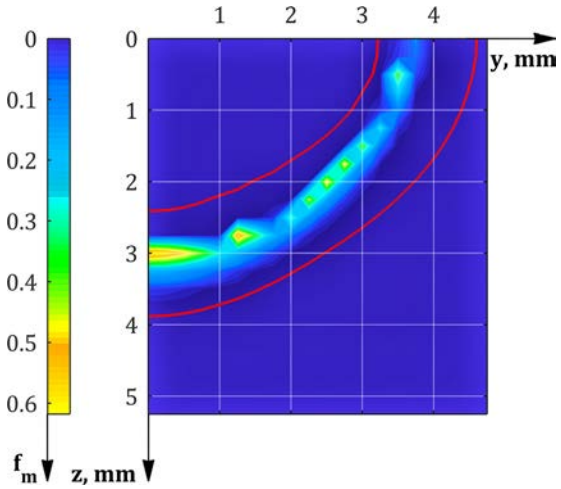

Figure 11: Simulation of martensite volume fraction

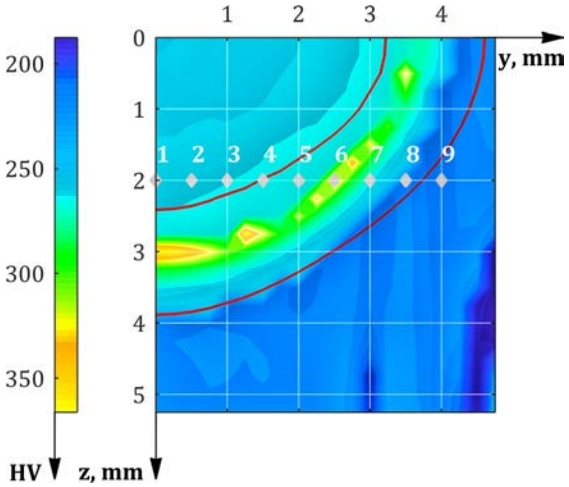

Figure 12: Simulation of Vicker’s hardness in weld cross section

7. EXPERIMENT

Dimensions of the P355GH welded steel sample were 300 x 150 x 5 mm, fig 13. Filler material used was OK Autrod 12.50 wire, with 1.0 mm diameter. As a shielding gas, we have used Arcal 5 (82%Ar + 18%CO2). Values of welding parameters were the same as in case of simulation.

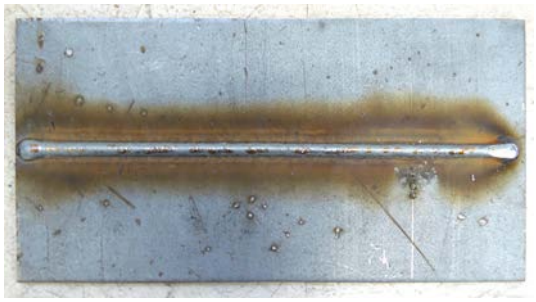

Figure 13: Welded sample

Fig. 14 shows comparision between simulated and experimental weld bead geometry while values of absolute and relative geometry of weld bead width – B, weld penetration – H, weld shape penetration factor – ψ are shown in table 3.

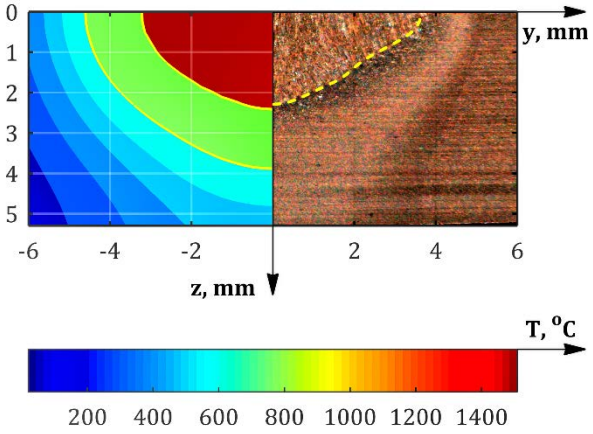

Figure 14: Comparison of simulated and experimental weld bead geometry

Table 3. Absolute and relative error of simulated weld bead geometry

Parameter	Unit of measurement	Absolute error	Relative error [%]
B	mm	0.83	11.4%
H	mm	0.09	4.1%
ψ = B/H		0.47	14.9%

Measurements of hardness were performed using Vickers method. Due to the small dimensions of the welded joint, the measurements were performed using a load of 9.81N. Hardness was measured in a series of points at a distance of 2 mm from the upper surface of the samples. The distance between the measuring points was 0.5 mm, fig 8.

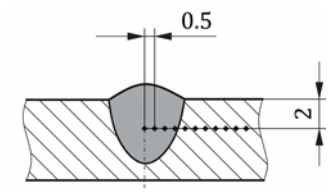

Figure 15: Location of indentations

We have made comparison of simulated and experimental values of hardness at identations which is shown at fig.16.

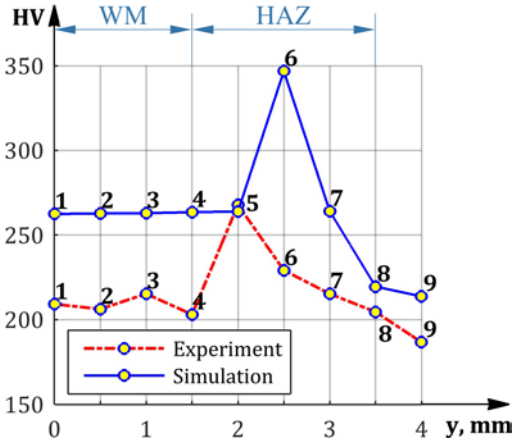

Figure 16: Comparison of simulated and experimental hardness at indentation points

Relative error of hardness simulation at identations is shown on fig. 17.

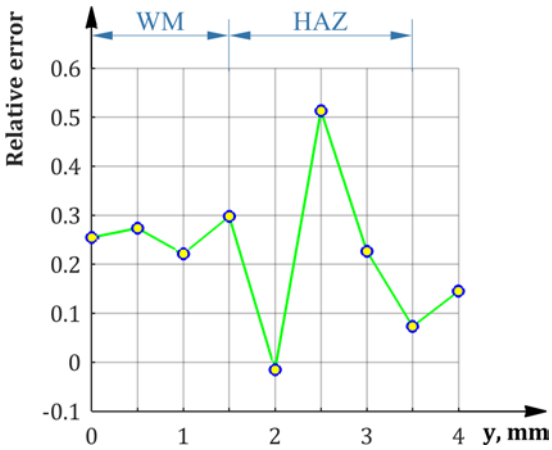

Figure 17: Relative error of simulation

8. SUMMARY AND CONCLUSIONS

In order to simulate hardness distribution at HAZ we have combined three dimensional model of heat transfer during welding with Kirkaldy's model of austenite decomposition. Results obtained by simulation are compared with experimental ones. In case of weld bead geometry results of simulation were in very good agreement with experimental results. Something larger deviations that occurred in case of hardness can be explained as a result of direct application of the metallurgical model without calibration. The calibration of the model could not be performed due to the lack of an experimentally obtained isothermal transformation diagram for the P355GH steel which could be used to adjust the parameters of the microstructural model. Presented method represents a good starting position for simulation of microstructure volume fractions and hardness in HAZ.

ACKNOWLEDGEMENTS

The authors wish to express their gratitude to National CEEPUS Office of Czech Republic (project CIII-HR-0108-07-1314) and to the Ministry of Education and Science of the Republic of Serbia (project TR37020).

NOMENCLATURE

- Ae_1 – lower equilibrium austenite formation temperature, [°C]
- Ae_3 – upper equilibrium austenite formation temperature, [°C]
- a_{hf} – semiaxis of front half-ellipse in x - direction, [m]
- a_{hb} – semiaxis of rear half-ellipse in x - direction, [m]
- B_s – bainite start temperature, [°C]
- b_h – semiaxis of front half-ellipse in y - direction, [m]
- c_p – specific heat, [$J \cdot kg^{-1} \cdot K^{-1}$]
- c_h – semiaxis of front and rear half-ellipse in z - direction, [m]
- f_b – bainite volume fraction
- f_p – pearlite volume fraction
- f_m – martensite volume fraction
- f_α – ferrite volume fraction
- g – grain size, [m]
- H – depth of penetration, [m]
- HV – Vicker’s hardness
- HV_B – Vicker’s hardness of bainite
- HV_{FP} – Vicker’s hardness of ferite and pearlite
- HV_M – Vicker’s hardness of martensite
- I – welding current, [A]
- k – grain growth constant, [mm^2/min]
- L – latent heat, [Jkg^{-1}]
- M_s – martensite start temperature, [°C]
- q_{lf} – power density in front quadrant, [Wm^{-3}]
- q_{lb} – power density in rear quadrant, [Wm^{-3}]
- R – universal gas constant, [$J \cdot mol^{-1} \cdot K^{-1}$]
- T – temperature, [°C]
- T_a – ambience temperature, [°C]
- T_{liq} – liquidus temperature, [°C]
- T_{sol} – lolidus temperature, [°C]
- U – arc voltage, [V]
- V_r – cooling speed at 700°C, [$°C \cdot s^{-1}$]
- v_z – welding speed, [$m \cdot s^{-1}$]
- X_F – normalized volume fraction of ferrite, [%]
- X_P – normalized volume fraction of pearlite, [%]
- X_B – normalized volume fraction of bainite, [%]
- $\Delta t_{8/5}$ – cooling time from 800 – 500°C
- λ – thermal conductivity, $W \cdot m^{-1} \cdot K^{-1}$
- τ – time, [s]
- τ_B – time to isotherm. transf. of austenite fraction to bainite, [s]
- τ_F – time to isotherm. transf. of austenite fraction to ferrite, [s]
- τ_P – time to isotherm. transf. of austenite fraction to pearlite, [s]
- ψ – weld bead width to depth ratio

REFERENCES

[1] D. Rosenthal, “Mathematical theory of heat distribution during welding and cutting”, Welding Journal. 20 (1941) 220s–234s.

[2] N.N. Rykalin, “Calculations of thermal processes in welding”, 1951.

[3] G. Xu, J. Hu, H.L. Tsai, “Three-dimensional modeling of arc plasma and metal transfer in gas metal arc welding”, International Journal of Heat and Mass Transfer. 52 (2009) 1709–1724.

[4] M. Schnick, U. Fuessel, M. Hertel, M. Haessler, A. Spille-Kohoff, A.B. Murphy, “Modelling of gas–metal arc welding taking into account metal vapour”, Journal of Physics D: Applied Physics. 43 (2010) 434008.

[5] Ø. Grong, “Metallurgical modelling of welding”, Institute of Materials, London, 1997.

[6] M. Bjelić, “Characterization of weld geometry and microstructure based on heat-transfer and metallurgical model of the GMAW process as a basis for prediction of the technological parameters”, University of Kragujevac, 2016.

[7] J. Kirkaldy, D. Venugopalan, “Prediction of microstructure and hardenability in low-alloy steels, in: International Conference on Phase Transformations in Ferrous Alloys”, 1983: pp. 125–148.

[8] J. Goldak, A. Chakravarti, M. Bibby, “A new finite element model for welding heat sources”, Metallurgical Transactions B. 15 (1984) 299–305.

[9] M. Bjelić, K. Kovanda, L. Kolařík, M. Vukićević, B. Radičević, “Numerical modeling of two-dimensional heat-transfer and temperature-based calibration using simulated annealing optimization method: Application to gas metal arc welding”, Thermal Science. 20 (2016) 655–665.

[10] C. Zener, “Kinetics of the decomposition of austenite”, in: Trans. AIME, 1946: pp. 550–595.

[11] M. Hillert, “The role of interfacial energy during solid state phase transformations”, Jernkontorets Annaler. 141 (1957) 757–789.

[12] J.A. Goldak, M. Akhlaghi, “Computational welding mechanics”, Springer, New York, 2005.

[13] P. Maynier, B. Jungmann, J. Dollet, “Creusot-Loire System for the Prediction of the Mechanical Properties of Low Alloy Steel Products”, Trans. AIME, 1977: pp. 518–545.

[14] M.F. Ashby, K.E. Easterling, “A first report on diagrams for grain growth in welds”, Acta Metallurgica. 30 (1982) 1969–1978.

[15] C.H. Gür, C. Şimşir, “Simulation of Quenching”, in: Handbook of Thermal Process Modeling of Steels, CRC Press, Boca Raton - Florida, 2009.